70th International Astronautical Congress (IAC), Washington D.C., United States, 21-25 October 2019

IAC-19/D2/6x49695

Numerical Crash Simulation of the Reusability Flight Experiment ReFEx

Waldemar Bauer [a], **Eduard Schnorr** [a], **Andreas Rittweger** [a], **Peter Rickmers** [a]

a) *German Aerospace Center (DLR), Institute of Space Systems, Robert-Hooke-Str. 7,28359 Bremen, Germany,* waldemar.bauer@dlr.de, eduard.schnorr@dlr.de, andreas.rittweger@dlr.de, peter.rickmers@dlr.de

Abstract

The Reusability Flight Experiment (ReFEx) is currently under development at the German Aerospace Center (DLR). The project passed the preliminary design review in Mai 2019 and the launch on a Brazilian VSB-30 sounding rocket is scheduled in 2022. The main goals of the project are the demonstration of a controlled autonomous re-entry flight from hypersonic velocity down to subsonic range and the testing of the *key technologies* required for *future reusable winged first stage systems*. Furthermore, the acquisition of the in-flight generated data is crucial for the Post Flight Analysis (PFA) as well as for the development of future reusable launch systems. As for the experimental vehicle no landing gear and no parachute has been foreseen, it will perform a hard touch down at the end of the mission. This issue needs to be considered in the vehicle design, since the memory units inside the vehicle needs to be recovered after the crash for the PFA. Therefore, an intensive investigation of possible crash scenarios has been performed to obtain preliminary assessment of the effect on the systems. This paper provides a mission and system overview. Furthermore, the preliminary analysis results as well as the corresponding assumptions regarding the crash analysis are outlined and discussed.

Keywords: *ReFEx, reusable first stage, launch vehicle*

1. Introduction

The German Aerospace Center (DLR) is currently developing a flight demonstrator in the frame of the Reusability Flight Experiments (ReFEx) project. The flight demonstration is planned for 2022. The experimental vehicle shall perform a controlled re-entry flight similar to that of full-scale winged reusable stages. The technological know-how shall enable an appropriate assessment of the Vertical Take-off and Horizontal Landing (VTHL) concept and support decisions regarding future launch systems development. The main goals of the ReFEx project are:

- *Perform a controlled flight following a re-entry trajectory representative for a winged RLV first stage in the velocity range hypersonic down to subsonic*
- *Perform a controlled heading change (capability required for returning to the launch site)*
- *Test of the autonomous Guidance Navigation and Control (GNC) system*
- *Perform In Flight Data acquisition using advanced sensors*
- *Recovery of the Re-Entry Segment (see Figure 2 right) for Post Flight Analysis (PFA)*

Since no soft landing systems (e.g. parachute, landing gear) are foreseen for this mission, the re-entry vehicle will perform a hard touch down (crash landing). Therefore, the final state of the Re-Entry Segment is difficult to predict. A preliminary crash analysis was performed to analyze the impact loads which serves as a basis for units design. The aim is to reduce the harm to the memories of the units by design and accommodation of the units.

2. System and Mission Overview

Figure 1 shows the ReFEx Launch Configuration and a section view of the Re-Entry Segment, called ReFEx. The integrated units are grouped to the following subsystems:

- Guidance Navigation and Control (GNC)
- Avionics (AVS)
- Structure (STR)
- Flight Instrumentation (FIN)

Figure 2 illustrates the Payload (to be placed on top of the VSB-30 sounding rocket as shown in Figure 1) as well as the Re-Entry Segment as foreseen for the re-entry flight. The VSB-30 has no active thrust vector control capabilities (passive stabilized system). Therefore, the Payload is required to have an almost rotationally symmetrical shape to enable a safe launch. However, the Re-Entry Segment needs to have an aerodynamic shape for the Experimental Phase (re-entry, see Figure 3) which is contradicting the launch requirement. To meet both requirements the wings of the experimental vehicle were designed foldable and are covered by a fairing for the atmospheric passage. The Re-Entry Segment has a length of 2.7 m, a wingspan of 1.1 m, a mass of approx. 400 kg and is a highly integrated system as can be seen in Figure 1. More details can be found in [1].

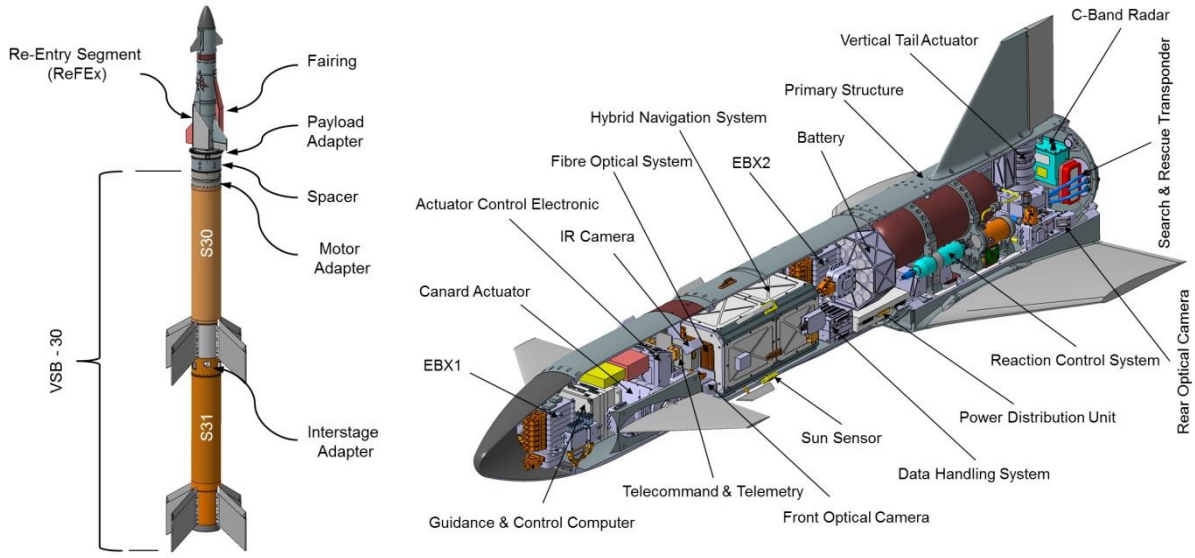

Figure 1: ReFEx Launch Configuration (left), section view of the Re-Entry Segment -ReFEx- (right)

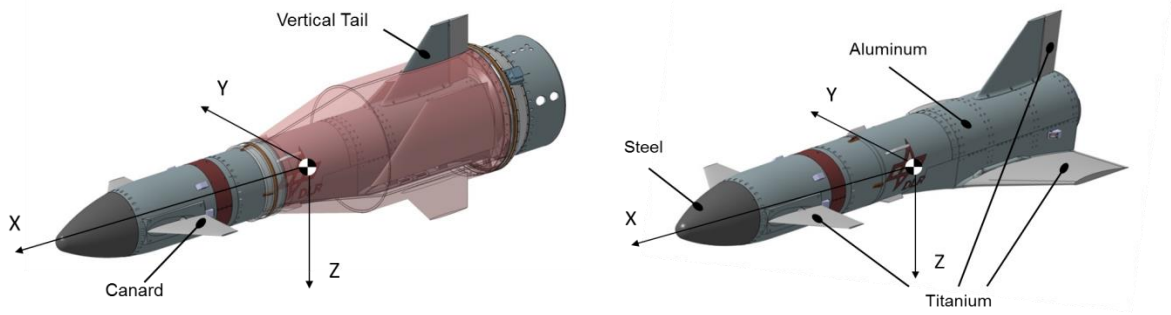

Figure 2: Configuration of the Payload (left) and the Re-Entry Segment (right)

Figure 3 shows schematically the flight profile for the ReFEx mission with preliminary details regarding time and altitudes. For the Launch Phase all elements which could potentially unintended influence the launch trajectory are locked. After the ignition of the first stage (S31) the ReFEx Launch Configuration will perform a Lift-Off. The first stage (S31) burns out and is separated at 12 s after ignition. About 20 s after launch, the second stage (S30) will be ignited. The S30 burn-out is at 49 s after launch. During the Launch Phase, the VSB-30 will build up a spin rate to compensate thrust inaccuracies. Therefore, the spin rate of the payload shall be reduced afterwards using a Yo-Yo system at 79 s. The fairing separation occurs at 84 s after launch. The wings are preloaded under the fairing during the Launch Phase. The corresponding mechanisms will deploy the wings together with the fairing release and lock the wings at the deployed position. Subsequently, the Re-Entry Segment will be separated from the payload adapter.

This particular point is called the *Separation Point (SEP)* of Re-Entry Segment. This is also the start of

the Experimental Phase and the *Beginning of Guided Control (BoGC)* of the vehicle. After Re-Entry Segment separation, the control elements (canards, rudder, Reaction Control System (RCS)) will be unlocked. The RCS reduces the remaining angular velocity of the Re-Entry Segment and performs required adjustments in the orientation to enable the vehicle to meet the *Entry Interface* (EI).

After passing the EI, the Re-Entry Segment control occurs via the RCS and the aerodynamic control surfaces (canards, rudder) in complementary manner until all nitrogen within the RCS tanks is consumed. The RCS system however contributes to the control of the vehicle effectively down to an altitude of approx. 50 km. As the atmosphere becomes denser at lower altitudes and the dynamic pressure rises, the vehicle is controlled by the aerodynamic control surfaces only.

The re-entry vehicle does not possess sufficient natural longitudinal and lateral stability in belly-down configuration for high Mach numbers (approx. Ma > 2.5). In order to avoid these unstable flight regimes, the vehicle performs a ballistic flight, entering the EI and the Reusable Launch Vehicle (RLV) corridor in belly-up orientation (vertical tail pointing downwards). In the range of Mach 2-1.5 the Re-Entry Segment performs a roll maneuver. After the roll, the vehicle remains in belly-down orientation for the rest of the mission. This maneuver is necessary, because the control effectiveness in belly-up orientation of the Re-Entry Segment decreases significantly with decreasing Mach number. Therefore the re-entry vehicle becomes increasingly unstable and not controllable. The aforementioned roll maneuver ensures sufficient natural stability and controllability of the vehicle throughout the mission. At an altitude of approx. 10 km the vehicle enters a dispersion ellipsoid which initiates the *End of Experiment* (EoE). To reduce the kinetic energy of the Re-Entry Segment prior to touch down a flare maneuver is envisaged at an altitude of approx. 120 m over the ground.

The telemetry (TM) data shall be transmitted to the ground stations (one at the launch site and one mobile ground station placed close to the expected landing location) at least to the point End of Experiment. However, possibilities will be investigated in the frame of the project to transmit the TM data down to the end. In this way, all data required for future developments will be transmitted to the ground stations during the flight. However, only a part of the total data will be transmitted because of the data link limitations. Therefore, the aim of the project is to recover the hardware after the experimental flight and to have access to the entire datasets of the units.

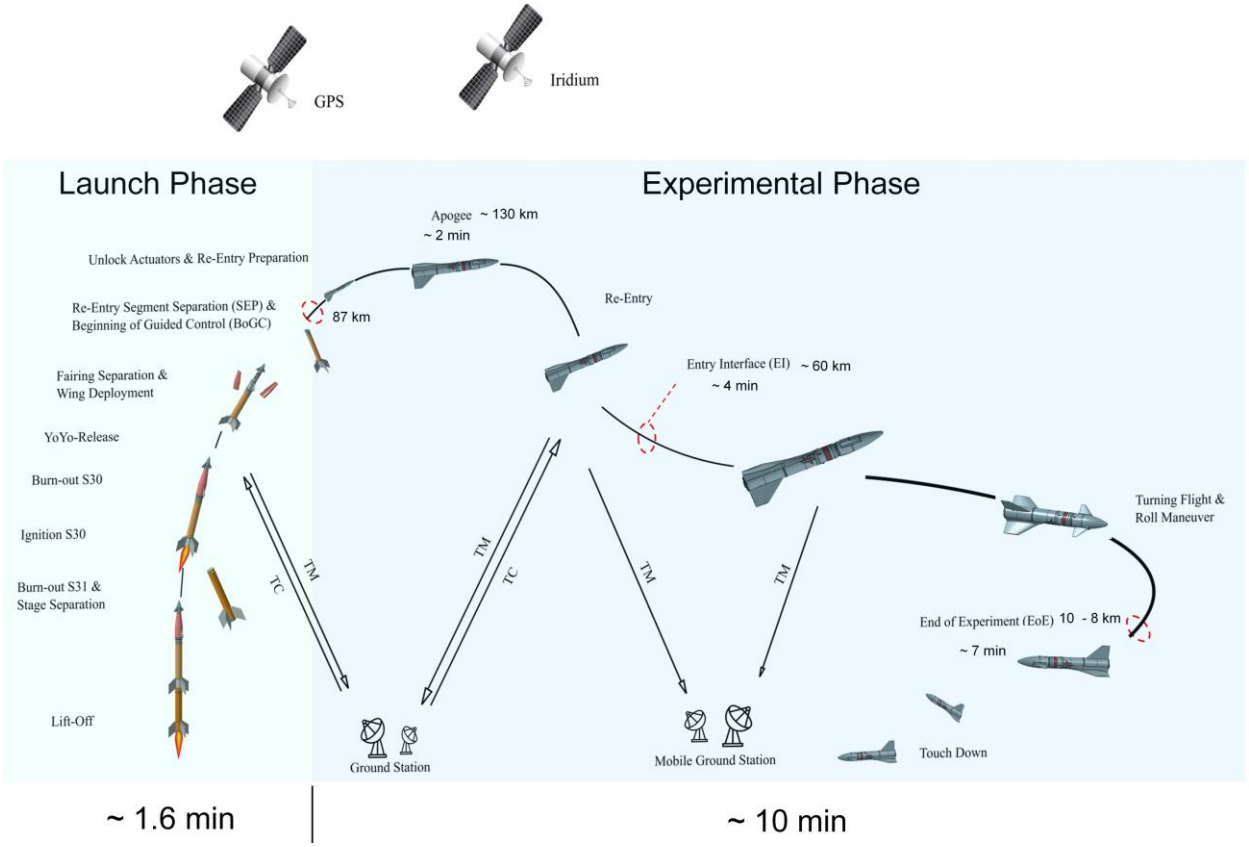

Figure 3: Mission Architecture & Flight Events

3. Crash Analysis Methodology

The collision of at least two objects with each other is a complex process, which depends on many factors such as mass and material properties of the objects, relative velocity, and geometry of the objects as well as of the collision. In the frame of product development, the highly dynamic crash process can be acceptable accessed in different ways.

One possibility is the conduction of experimental crash tests utilizing representative hardware and boundary conditions such as impact velocity and impact geometry. Since different impact scenarios are possible, a number of relevant tests need to be defined and performed. After testing, a hardware analysis regarding the damages needs to be conducted. The results of those analyses serve as an input for the design improvements of the tested hardware. Subsequently, the redesigned products undergo again experimental testing. As a rule, this approach is acceptable for small projects with low hardware cost and low number of tests. However, for larger projects such as for the aircraft or car industry this approach is not suitable because of high cost for hardware and testing procedures.

To reduce the number of required tests as well as the corresponding cost it is common to perform numerical crash simulations using the Finite Element Method (FEM) prior to hardware testing. The aim is to model the reality as accurately as possible using the numerical model considering the cost of the activity. However, due to a variety of interactions between the involved components of a vehicle as well as correct mapping of the material properties of the components, the numerical crash simulation is a very sophisticated task. In order to perform a numerical simulation, the FEM models needs to be appropriate simplified compared to the available CAD model. A CAD model contains e.g. detailed information, which has minor effect on simulation results but increases the computational effort significantly. Furthermore, the contact algorithms in-between the components need to be defined properly to simulate realistic behavior. Moreover, the material properties need to be defined. Especially the correct definition of the material properties is challenging, since the published data is rare. Hence, the responsible engineer needs to perform dedicated material testing or define the material properties based on data of comparable materials. Since most of the materials are strain rate dependent, the correct definition of the properties without testing is difficult. Therefore, a numerical model is generally error-prone. Finally, the numerical model quality assessment occurs by comparing numerical simulation with experimental results. An acceptable ratio of effort for numerical model development to achieved results depends highly on know-how of the responsible engineer.

To address the need of the ReFEx project an intensive research has been performed regarding already available experimental as well as simulated crash results. Subsequently FEM models were developed and appropriate verified against available data.

Figure 4 shows two examples comparing experimental crash with numerical simulation results. One example shows a Chevrolet Silverado which crashes against a concrete barrier. The mass of the vehicle is 2,270 kg [2], the impact velocity is 101 km/h [2] and the impact angle is 25.2° [2]. The experiment was performed in January 2009 [2] on the test site of the Texas Transportation Institute in the United States. Another example is an ATR42-300 regional aircraft that crashes on a concrete. The mass of the plane is 33.200 lb. [3] (15,059 kg) and the vertical velocity is 30 ft / s [3] (9,144 m / s). The drop test of the aircraft from an altitude of 14 ft. [3] (about 4.27 m) was performed on July 30, 2003 [3] on the test area of the Federal Aviation Administration (FAA) William J. Hughes Technical Center in the US.

These two examples show an acceptable compliance of the numerical simulation with the experimental results. In this way the developed FEM models adequately supports the experimental testing and product development.

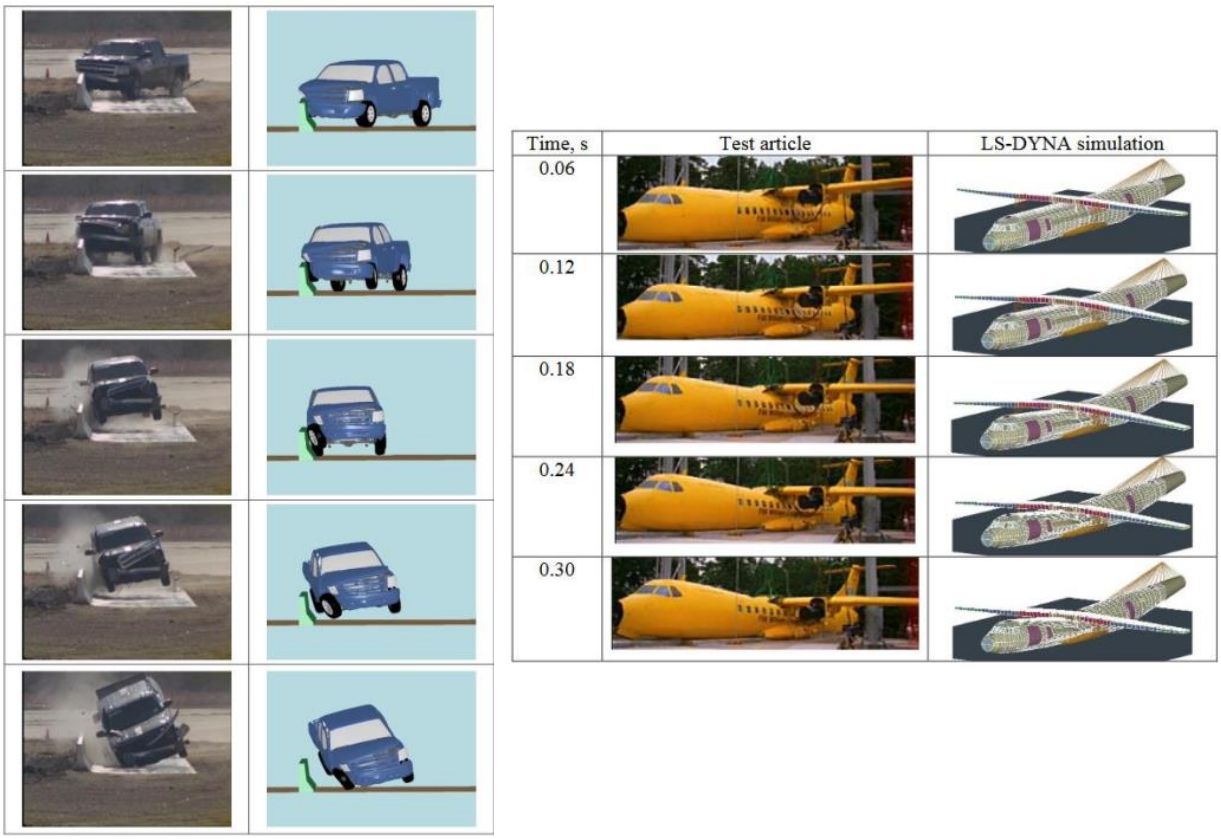

Figure 4: Comparison of numerical numerischen simulation results (using LS-DYNA) with experimental crash tests: Chevrolet Silverado [2] (left), ATR42-300 aircraft [3] (top right)

4. Models Overview

The general development process of the FEM models in the frame of the ReFEx project is shown Figure 5. The analysis is subdivided into two domains: the Re-Entry Segment Structure and the Impact Soil. The first step is the discretization of the vehicle structure. The individual components of the vehicles structure are defined as shell and solid elements and of the soil as solid and particle elements (Smoothed Particle Hydrodynamics, SPH). The allocation of material properties is followed by the discretization task. For the Re-Entry Segment the selected materials are aluminum, titanium and steel and the Impact Soil is defined as rigit and sand.

An appropriate modelling (types of finite elements, element size, and contact algorithms) was done based on numerical test cases performed in advance. The test cases were compared with each other as well as with the analytical results utilizing different modeling approaches. This comprises fuselage segments, interface rings, frames and stringers as well as the contacts between the fuselage segments and the fuselage segments and the interface rings. Furthermore, comparable experimental results were reproduced using numerical models.

The soil was defined as rigid for the worst case scenario. To investigate a more realistic crash behavior of the soil, a sand model was used. For a sandy soil, a comparison was performed between the FEM models and the SPH models. This helped to assess the suitability of the SPH model in the areas of high deformation (bottom vertical tail penetrates the sandy soil). The SPH model offers the advantage of not having a calculation grid. Such a grid can distort strongly in areas of very high deformation and thus leads to unrealistic results. However, within this paper only the rigid soil modeling is discussed. The final FEM model combines the Re-Entry Segment model and the Soil model to a single model for which the boundary conditions (e. g. impact velocity, impact geometry) can be defined.

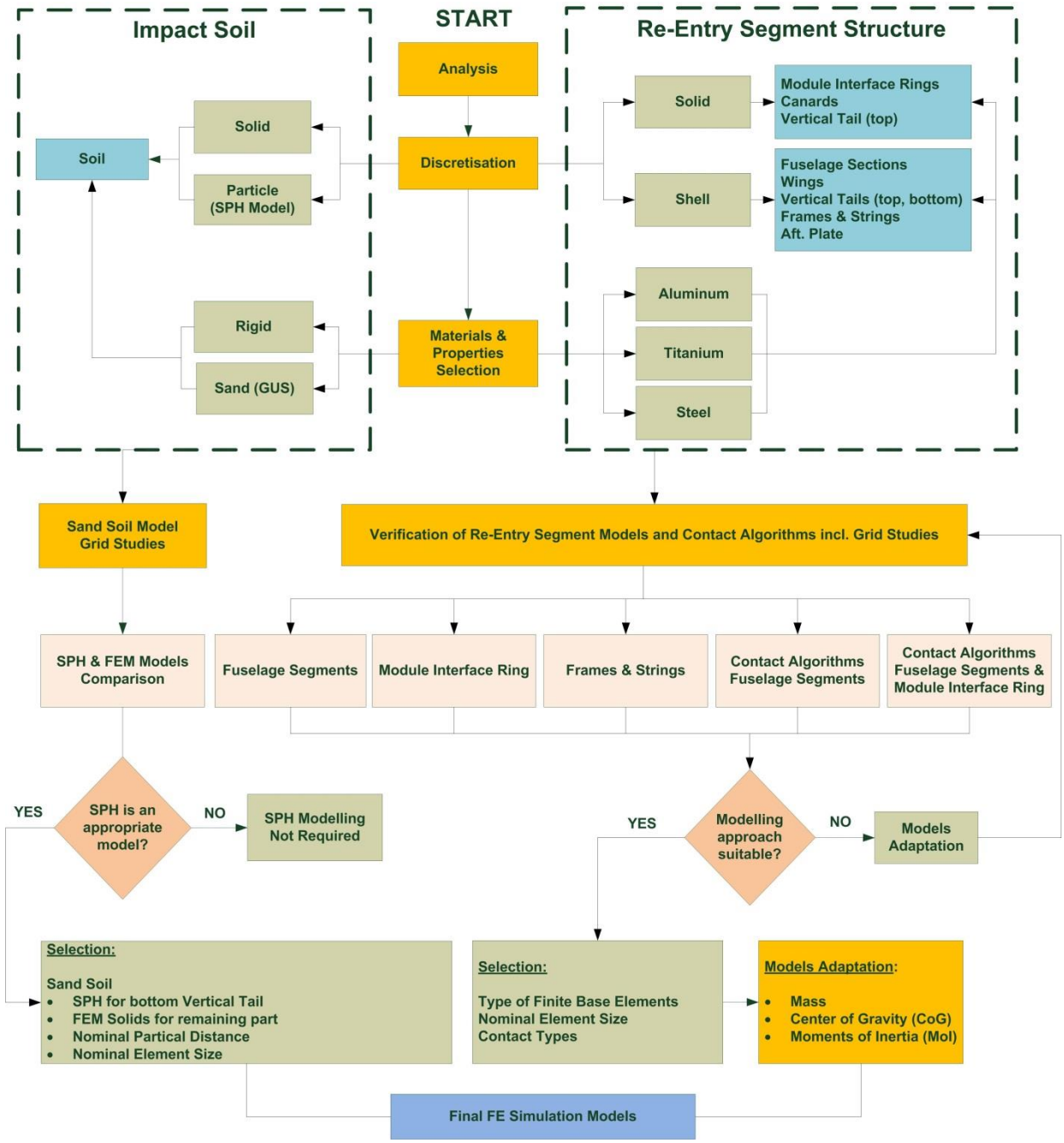

Figure 5: Schematic process overview of FEM simulation models selection

The preliminary crash analysis was performed for the primary structure of the Re-Entry Segment without internal systems (see Figure 1). Since the developed FEM model has a modular structure and enables modifications and extensions, the internal systems can be integrated into the FEM model subsequently to enable a more detailed crash analysis.

Two different configurations of the re-entry vehicle were analyzed, which are different regarding the vertical tails. Figure 6 shows the Configuration 1, which comprises top and bottom vertical tail. The Configuration 2 is designed without the bottom vertical tail and the top one is smaller than that of the Configuration 1 (see Figure 2, right). Figure 7 shows the discretized model.

The pre- and post-processing of the FEM models was done using LS-PrePost and the simulation was performed utilizing LS-DYNA. As mentioned above the structure of the vehicle was simplified prior to discretization activity. Hence, the holes were removed as they do not significantly contribute to the structural strength but increases grid generation and computation effort. Furthermore, the pockets of the Fuselage Sections (FS), as well as the groove for the

connection of Re-Entry Segment to the fairing of the VSB-30 are not considered. The canards are attached directly to the fuselage without the spacer in-between the fuselage and the canards (compare Figure 6 and Figure 7). The Re-Entry Segment is stiffened by stringers (longitudinal stiffeners) and frames (radial stiffeners). The radially closed frames are denoted as "interface rings" and the half-open as “frames”. The partly rectangular and partly circular closed frame in the rear of the structure are also denoted as "interface rings".

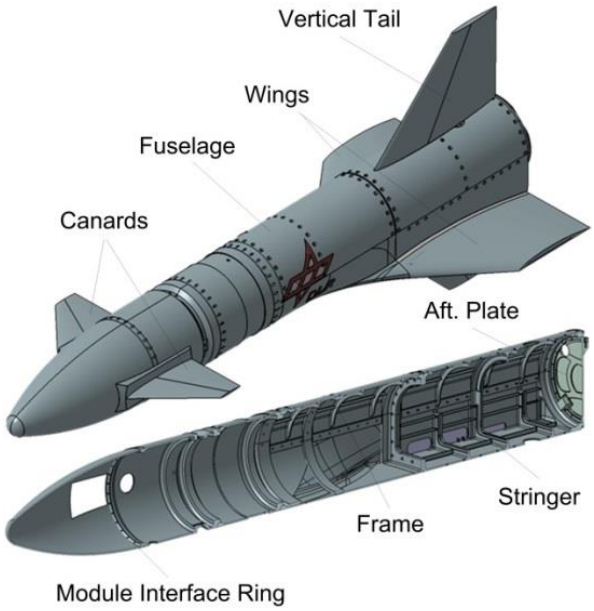

Figure 6: Re-Entry Segment CAD Model (configuration 1)

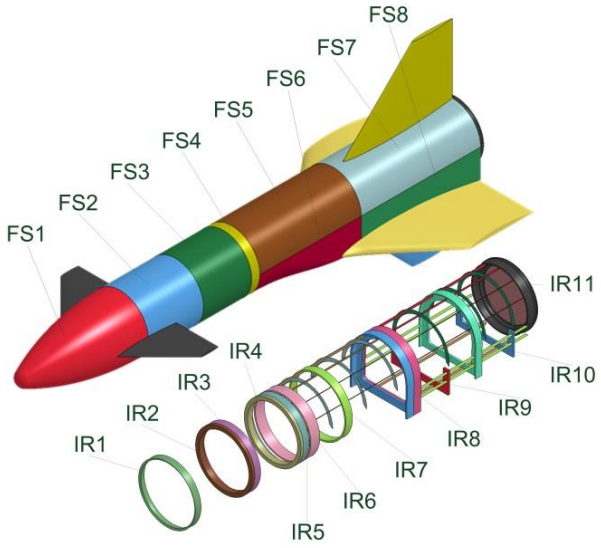

Figure 7: Re-Entry Segment FEM model, FS = Fuselage Section, IR = Interface Ring (Configuration 1)

The structure modeling was performed using solids and shells. The shells are suitable for thin-walled components of the structure and the solids for thick-walled components and solid bodies. The skin of each Fuselage Section (FS) is modeled as shells and the interface rings as solids. Some of the interface rings are designed as an integral part of the FS in CAD model (see Figure 6). Those interface rings were separated from the FS, modeled as solid elements and subsequently rigidly connected with contact algorithms to the skin. In this way only the interface rings are modeled as solids but not the whole fuselage section, which significantly decreases the calculation time. The stringers and frames are modeled as shells. The thin-walled components (wings, after plate and lower vertical tail in Configuration 1 and upper vertical tail in Configuration 2) are modeled as shells according to the modeling of the fuselage sections. The solid bodies (canards, upper vertical tail in Configuration 1 and the u-shaped stiffening elements between IR9 and IR10 and RR10 and IR11) are modelled as solids.

The FEM model of the Configuration 1 consists of 1,092,658 nodes, 207,724 shells, and 697,028 solids. The Configuration 2 differs slightly from Configuration 1 with 1,069,129 nodes, 199,824 shells, and 685,805 solids. The shell modelling was done using ELFORM 16 and the solid using ELFORM 2. The soil was assumed to be rigid and was modeled with ELFORM 1.

The contact between the fuselage sections is defined as TIED_SHELL_EDGE_TO_SURFACE. The contact between the fuselage sections and the interface rings, stringers and frames, as well as the contact between the fuselage sections and the wings, the canards, the vertical tails is defined as TIED_SHELL_EDGE_TO_SURFACE_BEAM_OFFSET. The contact between the soil and the structure is modelled as AUTOMATIC_NODES_TO_SURFACE with a friction coefficient of 0.5. This value is selected based on studies of Tsubakihara et al. [4], who have studied the coefficient of friction between different sandy soils and steels with different surface roughness. Crash simulations are expected to cause large deformations. As a result, the number of contacts increases in-between components as well as self-contact of parts due to strong compression (e.g. fuselage sections). For these reasons, a global contact AUTOMATIC_SINGLE_SURFACE is defined with a coefficient of friction of 0.2, which ensures that components cannot penetrate neither themselves nor other components.

The selection of the contact types and types of the finite elements are based on analysis results performed in advance. For example several fuselage sections were crushed in-between two rigid plates. The results were than compared and evaluated with the analytical model of DeRuntz und Hodge [5]. Furthermore, different contact conditions were investigated by impacting two connected fuselage sections with a defined velocity on a rigid plate and compared with the result of a geometrically identical fuselage section designed as one single piece. Subsequently, the contact conditions were assessed regarding inconsistencies and non-plausible deformations. Additionally, an intersection ring was integrated into a fuselage section and crushed between two rigid plates to determine best suitable contact type in-between the interface ring, stringer and the fuselage section skin (see Figure 8). The contacts were again examined for inaccuracies and implausible deformations. The friction in-between the structure and the ground was set to 0.5.

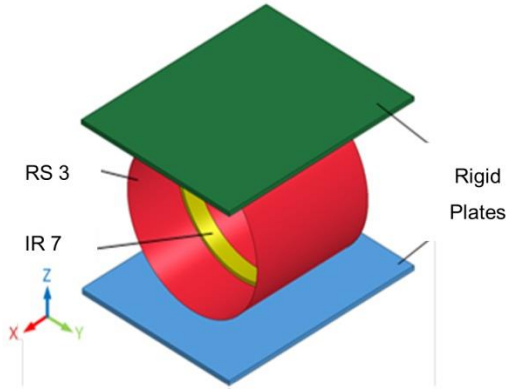

Figure 8: Behavior analysis: Crush of a frame reinforced fuselage sections in-between two plates.

The structure of the Re-Entry Segment consists of steel, aluminum and titanium parts. For the FEM analysis the alloys A36 (steel), AA6082-T6 (aluminum) and Ti6Al4V (titanium) were selected. The FS1 is made of steel. The fuselage sections FS2, FS3, FS5, FS7, the stringers and frames in FS 5 and FS7, the interface ring IR1 - IR4 as well as the top vertical tail in Configuration 1 are made of aluminum. The remaining components are made of titanium. In addition, the FEM model was adjusted to the CAD model regarding the moments of inertia and the total mass of the structure (without internal systems) by adding virtual point masses to the nodes.

Figure 9 the utilized impact geometry for the crash analysis of the Re-Entry Segment.

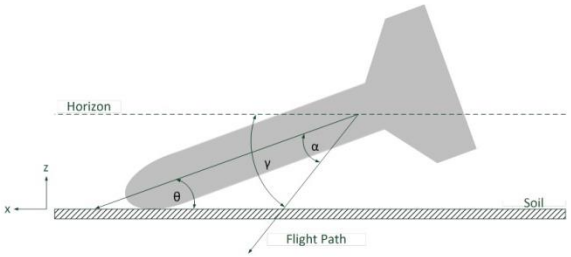

Figure 9: Impact geometry: α = angle of attack; γ = flight path angle; Θ = impact angle, v = velocity.

The crash simulations were performed using four different scenarios. Those scenarios are based on the aerodynamic database developed in the frame of the ReFEx project.

- Scenario 0: Impact at θ = 13°. To reduce the kinetic energy of the Re-Entry Segment, a flare maneuver shall be performed just before the touch down.
- Scenario 1: Impact at θ = -5°.
- Scenario 2: Impact at θ = -27°.
- Scenario 3 Impact at θ = -90°. The Re-Entry Segment enters the ground with the nose first (frontal collision).

Table 1: Defined scenarios for crash analysis

Scenario	γ (°)	α (°)	θ (°)	$\lvert v_{ges}\rvert$ (m/s)	$\lvert v_x\rvert$ (m/s)	$\lvert v_z\rvert$ (m/s)	$\lvert v_y\rvert$ (m/s)
0	2	11	13	100	100	3.5	0
I	-15	10	-5	145	140	37.5	0
II	-27	0	-27	270	240	122.6	0
III	-90	0	-90	70	0	70	0

5. Preliminary Simulation Results

Since scenario 0 shows minor deformations the description within this paper focuses on the scenarios I-III only where significant deformations of the structure can be expected. Figure 10 shows the deformation results of the Configuration 1 for the three defined scenarios (see Table 1) and Figure 11, Figure 12 and Figure 14 the deceleration of the corresponding Fuselage Sections during the collision. Some Fuselage Sections (FS) are summarized to Section (see Figure 10 and Figure 15, S1 – S4) to simplify the description of the analysis results.

In scenario I, the deformations occur mainly on the lower side of S1 and S2, as well as on the bottom vertical tail (see Figure 10, I). The Re-Entry Segment hits the ground with the bottom vertical tail first. Subsequently the fuselage rotates around the deforming vertical tail and impacts with the nose on the ground. The S1 impacts therefore with highest velocity on the ground due to the additional accelera-

tion because of the rotation. The corresponding deceleration due to the impact of S1 was analyzed to be approx. 2,400 g as shown in Figure 11. The rear shows lower decelerations of approx. 1,100 g.

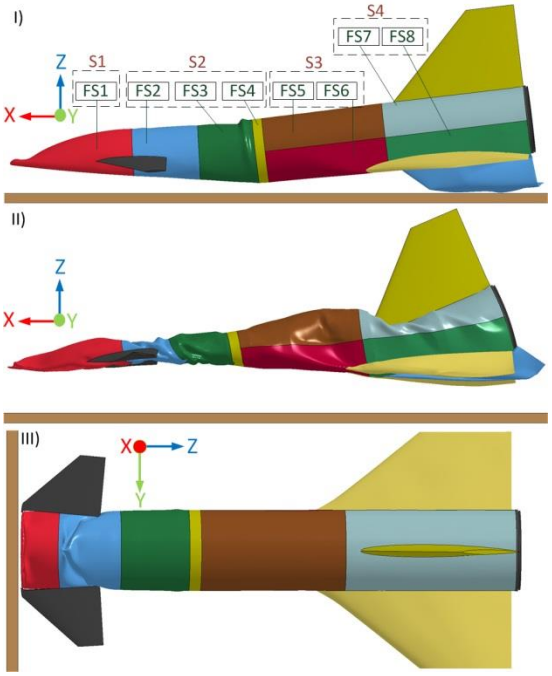

Figure 10: Configuration 1, impact on Rigid Soil
S=Section, FS=Fuselage Sections

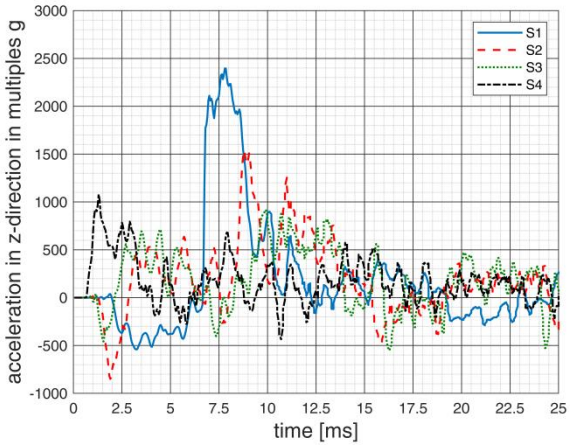

Figure 11: Time-dependent acceleration in multiples of g (Configuration 1, scenario 1)

The structural deformations in scenario II are the largest compared to the other scenarios (see Figure 10, II) and comprises all Fuselage Sections. The S1 and S2 are almost completely compressed and S2 shows wrinkles in FS2 and FS3. The S3 shows the smallest overall deformation since the vertical tail pushes FS7 in. Especially the area behind IR9 is strongly crushed. The deformations at the rear are smaller compared to the forward part because the stiffness of the structure at the rear is higher. The deformations of IR8, IR9 and IR11 at the rear part of the structure are small because of their high structural stiffness. In total, the FS8 maintained best of all Fuselage Sections. The FS8 has a stiff design (see also Figure 7) and, in contrast to FS7, it is made of titanium alloy instead of aluminum alloy. The highest deceleration in this scenario occurs at the rear part of the body because the nose impacts the ground first (deceleration maximum of the nose approx. 7,000 g). The structure again rotates around the deforming nose and the rear part accelerates to a higher impact velocity. In addition, the rear part of the structure is stiffer and less yielding which leads to a lower damping and high deceleration up to 10,000 g.

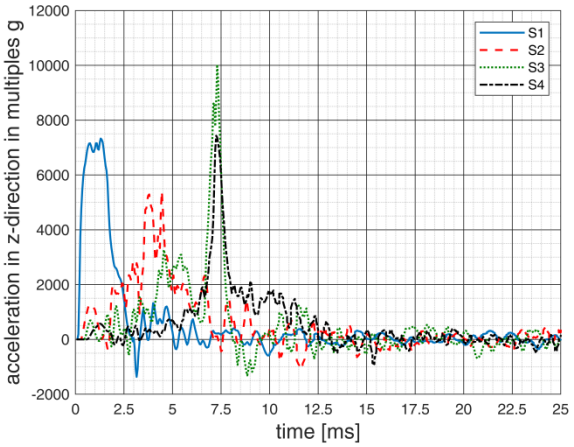

Figure 12: Time-dependent deceleration in multiples g (Configuration 1, scenario II)

In scenario III, the highest deformation of the structure occurs on FS1 and FS2 (see Figure 10, III). Figure 13 shows the FS1, which is compressed by a multiple transverse fold formation. This process transforms a significant portion of the kinetic energy into plastic deformation of the structure. The time-dependent deceleration curve (see Figure 14) is strongly influenced by the transverse fold formation process of FS1. All sections show an oscillating deceleration course of the curves. This characteristic is similar to the oscillating force curve in a folding absorber used e.g. as a bumper in the car industry. The largest deceleration of 7,800 g occurs at S1.

Figure 13: Deformed FS1 of Configuration 1

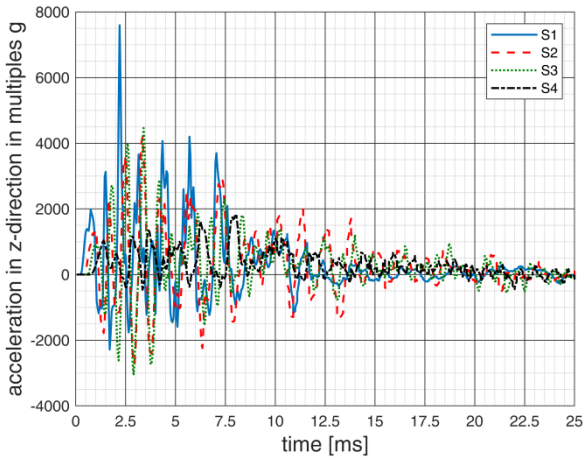

Figure 14: Time-dependent deceleration in multiples of g (Configuration 1, scenario III)

Figure 15 shows the deformation results of the Configuration 2 for the three defined scenarios (see Table 1) and Figure 16, Figure 17, Figure 18 the deceleration of the corresponding Fuselage Sections during the collision.

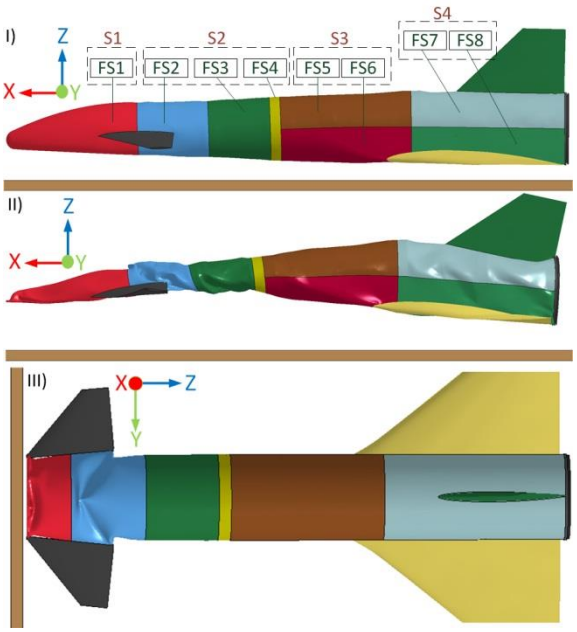

Figure 15: Configuration 2, impact on Rigid Soil S=Section, FS=Fuselage Sections

In scenario I, the deformations occur mainly at S1 and S2 (comparable to the Configuration 1). Due to the absence of a the bottom vertical tail, the nose part impacts the ground first and initiates rotation of the structure. The rear part of the structure impacts again with high velocity on the ground. Furthermore, because of absence of the lower vertical tail, the kinetic energy of the impacting body is higher, since no deformation on vertical tail was performed. Hence, the expected deceleration is approx. 9,000 g at the rear part and thus significantly higher than in Configuration 1.

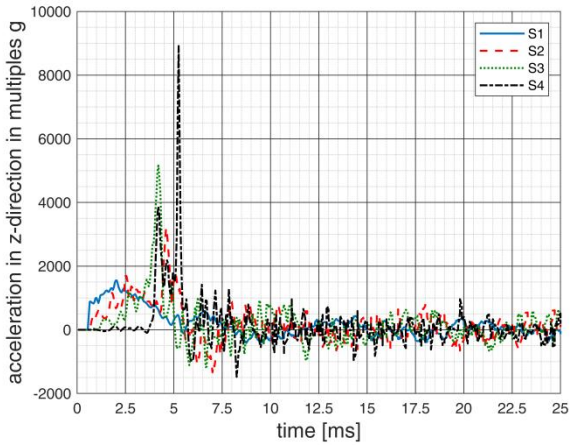

Figure 16: Time-dependent deceleration in multiples of g (Configuration 2, scenario I)

The structural deformations in scenario II are the largest (compare to Configuration 1) in contrast to the other scenarios (see, Figure 15, II). The S1 and S2 are almost completely compressed. The S3 at the front area is also mainly compressed. In the area of IR8 and IR9, the deformations are again the lowest which correlates to that of Configuration 1. The upper vertical tail presses the FS7 in. Both Configurations 1 and 2 impact the ground with the nose first. However, the lower vertical tail causes different deformations in the rear part of the structure. In case of Configuration 1, the upper vertical tail deforms the front area of FS7. Because of absence of the lower vertical tail on Configuration 2 the upper vertical tail crushes the rear area of FS7. However, the vertical tail of the Configuration 2 is thin-walled, smaller in dimensions and has therefore lower mass (although titanium alloy is used instead of aluminum alloy), so that the deformations of FS7 are smaller compared to the FS7 of the Configuration 1. Finally, the S4 has the lowest total deformations and the FS8 keeps the original shape best (like in Configuration 1).

The nose part hits the ground first and the S1 experiences a deceleration of approx. 7,500 g. The largest decelerations can be observed at S4. This is again due to the rotational related acceleration as well as and the higher structural stiffness of the rear part. Due to the absence of the lower vertical tail, the deceleration is approx. 18,000 g and is almost twice as high compared to Configuration 1.

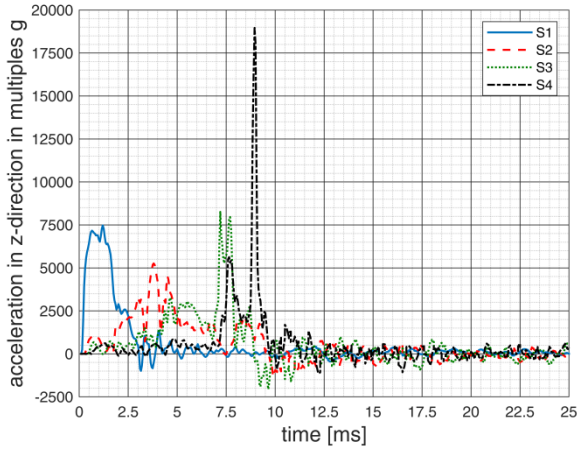

Figure 17: Time-dependent deceleration in multiples of g (Configuration 2, scenario II)

The deformation patterns of Configuration 2 in scenario III differs only slightly from those of Configuration 1. The deformations again occur mainly at FS1 and FS2. The FS1 is compressed by multiple transverse folds (see Figure 15, III) and thereby transforms most of the kinetic energy into the plastic deformation of the forward part of the structure. The deceleration curve shown in Figure 18 has the same characteristic as that of Configuration 1 (see Figure 14). The maximum deceleration of approx. 6,200 g is slightly lower than that of Configuration 1, which is mainly caused by the lower structural mass of Configuration 2.

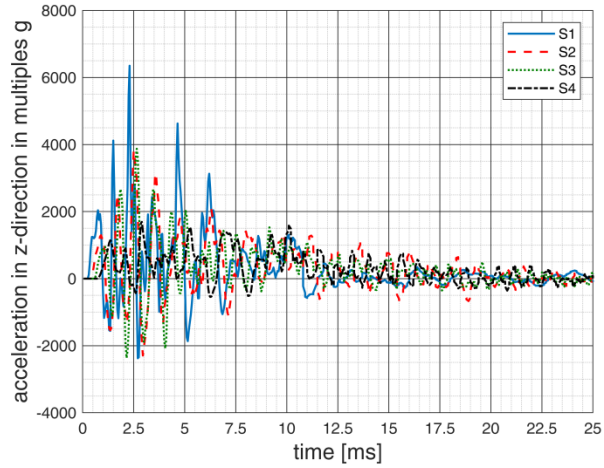

Figure 18: Time-dependent deceleration in multiples of g (Configuration 2, scenario III)

6. Conclusion / Outlook

This paper provides an overview of the DLR Reusability Flight Experiment (ReFEx) mission and addresses the finals stage of the mission. During the launch and experimental phases the in-flight generated data will be transmitted to the ground stations. Furthermore, the experimental vehicle will be recovered after flight for Post Flight Analysis (PFA). In this way the recovered memories of the systems serves as buck ups for the in-flight data. The main aim of the performed crash analysis is an appropriate loads and deformation prediction to the vehicle systems. The results support the development of systems and decrease the damage risk to the memory units.

7. References

[1] Bauer, W., Rickmers, P., Kallenbach, A., Stappert, S., Wartemann, V., Merrem, C. H-J., Schwarz, R., Sagliano, M., Grundmann, J. T., Flock, A., Thiele, T., Kiehn, D., Bierig, A., Windelberg, J., Ksenik, E., Bruns, T., Ruhe, T., Elsäßer, H., "DLR Reusability Flight Experiment ReFEx," *Acta Astronautica (under review)*.

[2] Marzougui, D., Kan, C.D., Opiela, K.S., "rash Test & Simulation Comparisons of a Pickup Truck & a Small Car Oblique Impacts Into a Concrete Barrier," in *Crash Test & Simulation Comparisons of a Pickup*, Detroit, Michigan, USA, 2014.

[3] Jackson, K., E., Fasanella, E. L., "Development of an LS-DYNA Model of an ATR42-300 Aircraft for Crash Simulation," in *8th International Users LS-DYNA Conference*, Detroit, Michigan, USA, 2004.

[4] Y. TSUBAKIHARA, H. KISHIDA, and T. NISHIYAMA, "Friction between cohesive soils and steel," *SOILS AND FOUNDATIONS*, vol. 33, no. 2, pp. 145–156, 1993.

[5] J. A. DeRuntz and P. G. Hodge, "Crushing of a Tube Between Rigid Plates," *J. Appl. Mech.*, vol. 30, no. 3, p. 391, 1963.